

# Raman Images of a Single Molecule in a Highly Confined Plasmonic Field

Sai Duan,<sup>1,2</sup> Guangjun Tian,<sup>2</sup> Yongfei Ji,<sup>2</sup> Jiushu Shao,<sup>3</sup> Zhenchao Dong,<sup>1</sup> and Yi Luo<sup>1,2,\*</sup>

<sup>1</sup>*Hefei National Laboratory for Physical Science at the Microscale and Synergetic Innovation Center of Quantum Information & Quantum Physics, University of Science and Technology of China, Hefei, 230026 Anhui, P. R. China.*

<sup>2</sup>*Department of Theoretical Chemistry and Biology, School of Biotechnology, Royal Institute of Technology, S-106 91 Stockholm, Sweden.*

<sup>3</sup>*Key Laboratory of Theoretical Computational Photochemistry, Ministry of Education, College of Chemistry, Beijing Normal University, Beijing 100875, P. R. China.*

(Dated: March 24, 2015)

Under the local plasmonic excitation, the Raman images of a single molecule can now reach sub-nanometer resolution. We report here a theoretical description of the interaction between a molecule and a highly confined plasmonic field. It is shown that when the spatial distribution of the plasmonic field is comparable with the size of the molecule, the optical transition matrix of the molecule becomes to be dependent on the position and the spatial distribution of the plasmonic field, resulting in spatially resolved Raman image of a molecule. It is found that the resonant Raman image reflects the electronic transition density of the molecule. In combination with the first principles calculations, the simulated Raman image of a porphyrin derivative adsorbed on the silver surface nicely reproduces its experimental counterpart. The present theory provides the basic framework for describing linear and nonlinear responses of molecules under the highly confined plasmonic field.

The development of tip enhanced Raman scattering (TERS) technique has significantly increased the spatial resolution of Raman images for molecules[1–3]. Under the low temperature and ultrahigh vacuum conditions, the resolution has amazingly reached a sub-nanometer level for a porphyrin derivative adsorbed on the silver surface[3]. It is anticipated that the spatial confinement of the tip-induced plasmon has played a decisive role in achieving such a high resolution. In this case, the spatial distribution of the plasmonic field has to be comparable with the size of the molecule, even with the inclusion of possible nonlinear processes[3]. This situation presents a great challenge to the conventional theory, which always assumes that the electromagnetic (EM) field uniformly interacts with the molecule[4]. A new theory that takes into account the locality of the EM thus needs to be developed. Moreover, what a Raman image really tells about the molecular structure is another important issue that has not yet been discussed in the literature.

In this work, we have derived a theoretical framework to describe Raman images of a molecule as observed in the TERS experiments. In combination with the first principles calculations, we have successfully reproduced experimental Raman image of the porphyrin derivative adsorbed on the silver surface. It is found that within the Born-Oppenheimer approximation, the resonant Raman image reflects the density of the electronic transition between the ground and the excited states. The role of linear and nonlinear processes on the resolution of the Raman images has been identified.

In the TERS experiments, a nano-cavity formed in-between the tip and the substrate is the host of the spatially confined plasmon (SCP). For the metals used in the experiments, the plasmonic frequency often falls into

the visible or ultraviolet-visible region, hence the electric dipole approximation[5] can still hold. The interaction Hamiltonian between SCP and adsorbates could be described by[5]

$$\mathcal{H}' = -e\hat{\mathbf{r}} \cdot \hat{\mathbf{E}}(\mathbf{r}, \mathbf{R}_T, t), \quad (1)$$

where  $e$  is the elementary charge,  $\hat{\mathbf{r}}$  is the electron position operator and  $\hat{\mathbf{E}}$  is the operator for electric field of SCP which is obviously related to the tip position  $\mathbf{R}_T$ . In this case,  $\hat{\mathbf{E}}$  cannot be treated uniformly in space due to its specific spatial distribution. Consequently, the optical transition matrix element between two states is determined by  $\langle\psi_g|\hat{\mathbf{r}}\hat{\mathbf{E}}(\mathbf{r}, \mathbf{R}_T)|\psi_r\rangle$  rather than  $\langle\psi_g|\hat{\mathbf{r}}|\psi_r\rangle$  as in the conventional response theory[6, 7]. This modification implies that the optical processes would be dependent on the position of the tip that hosts the SCP. This can naturally explain why it is possible to obtain super-high spatial resolution of the Raman images.

By taking into account the position dependent electric field, we can re-derive the expression for the spontaneous resonant linear Raman processes following the Albrecht's theory[4, 6]. The amplitude of induced linear polarization could be calculated as the summation of Franck-Condon (FC,  $A$ ) and Herzberg-Teller (HT,  $B$ ) terms,

$$\mathbf{P}_0^L = \mathbf{P}_{0,A}^L + \mathbf{P}_{0,B}^L, \quad (2)$$

where

$$\begin{aligned} \mathbf{P}_{0,A}^L = & \frac{\sqrt{F_P} M_i E_i^0}{\hbar} \left[ \langle\psi_g|\hat{\mathbf{r}}|\psi_r\rangle \langle\psi_r|\hat{\mathbf{r}}g(\mathbf{r}, \mathbf{R}_T)|\psi_g\rangle \right. \\ & \times \sum_{v^r=0}^{\infty} \frac{\langle v^f|v^r\rangle \langle v^r|v^i\rangle}{\omega_{e^r v^r: e^g v^i} - \omega_p - i\Gamma} \left. \right] + \text{NRT} \end{aligned} \quad (3)$$

$$\begin{aligned}
P_{0,B}^L = & \frac{\sqrt{F_P} M_i E_i^0}{\hbar} \left[ \frac{\partial \langle \psi_g | \hat{\mathbf{r}} | \psi_r \rangle}{\partial Q_k} \langle \psi_r | \hat{\mathbf{r}} g(\mathbf{r}, \mathbf{R}_T) | \psi_g \rangle \right. \\
& \times \sum_{v^r=0}^{\infty} \frac{\langle v^f | Q_k | v^r \rangle \langle v^r | v^i \rangle}{\omega_{e^r v^r: e^g v^i} - \omega_p - i\Gamma} \\
& + \langle \psi_g | \hat{\mathbf{r}} | \psi_r \rangle \frac{\partial \langle \psi_r | \hat{\mathbf{r}} g(\mathbf{r}, \mathbf{R}_T) | \psi_g \rangle}{\partial Q_k} \\
& \left. \times \sum_{v^r=0}^{\infty} \frac{\langle v^f | v^r \rangle \langle v^r | Q_k | v^i \rangle}{\omega_{e^r v^r: e^g v^i} - \omega_p - i\Gamma} \right] + \text{NRT}.
\end{aligned} \quad (4)$$

Here  $F_P$  is the Purcell factor[8] which accounts for the enhancement of spontaneous emission in nano-cavity and is independent on the position of the TERS tip in the  $xy$  plane,  $E_i^0$  is the electric field amplitude of incident laser,  $M_i$  is the enhancement factor of the SCP with respect to the incident laser,  $\hbar$  is the reduced Planck constant,  $|\psi_g\rangle$  and  $|\psi_r\rangle$  are the electronic ground and resonant excited states,  $g$  is the corresponding distribution function of the electric field amplitude of the SCP with proper normalization,  $Q_k$  is the corresponding normal mode,  $|v^i\rangle$  and  $|v^f\rangle$  are the initial and final vibrational states in  $|\psi_g\rangle$ ,  $|v^r\rangle$  is the vibrational state in  $|\psi_r\rangle$ ,  $\omega_{e^r v^r: e^g v^i}$  is the frequency difference between  $|\psi_r\rangle|v^r\rangle$  and  $|\psi_g\rangle|v^i\rangle$ ,  $\omega_p$  is the frequency of the plasmon generated by the incident light,  $\Gamma$  is the damping factor, and NRT is the non-resonant term. From the polarization, the Raman intensity can be calculated directly as[4, 6, 9]

$$I_s = \frac{\pi^2 c \tilde{\nu}_s^4 M_d^2 |P_0^L|^2}{2\epsilon_0}, \quad (5)$$

where  $c$  is the speed of light,  $\tilde{\nu}_s$  is the wave number of scattering,  $\epsilon_0$  is the permittivity of free space, and  $M_d$  is the directional radiation pattern factor[10]. Here the total polarization was treated as a classical oscillating dipole[9]. We have noted that the present consideration of SCP is equivalent to the quantization scheme proposed by Archambault *et al.*[11] for the propagation of the surface plasmonic waves as well as the classical treatment proposed by Xu and co-workers[12, 13]. The key difference here is to consider the effects of the distribution function  $g$  to the optical transition matrix. It should also be mentioned that the first order Taylor expansion for  $g(\mathbf{r}, \mathbf{R}_T)$  would naturally account for the electric field gradient effects in Raman spectroscopy as discussed in the literature[14–16].

For the sake of computations, we have chosen to expand the function  $g$  in terms of the Gaussian basis sets

$$g(\mathbf{r}, \mathbf{R}_T) = \sum_D \sum_{l,m,n} \sum_{\alpha} c_{\alpha,D}^{lmn} g_{\alpha,D}^{lmn}, \quad (6)$$

where  $g_{\alpha,D}^{lmn}$  is a Gaussian function localized at the center  $\mathbf{r}_D$  with exponent  $\alpha$ , which can be written as

$$g_{\alpha,D}^{lmn} = (x - x_D)^l (y - y_D)^m (z - z_D)^n e^{-\alpha(\mathbf{r} - \mathbf{r}_D)^2} \quad (7)$$

and  $c_{\alpha,D}^{lmn}$  is the corresponding coefficient. Here  $\mathbf{r}_D$  may represent the position of the SCP, which could be obtained by fitting the realistic electric field distribution and in principle it is not necessarily equal to  $\mathbf{R}_T$ . As the first demonstration, only the  $s$ -type Gaussian functions are considered for  $g_{\alpha,D}^{lmn}$ . It is noted that for absolute Raman intensities  $g$  should satisfy some proper normalization conditions. However, for the Raman images, the relative values are adequate. For the practical calculations, we chose  $c_{\alpha,D}^{lmn} = 1$  and  $l = m = n = 0$  in Eq. 6. Moreover, for a molecule under the TERS tip, only the  $zz$  component needs to be evaluated[3].

We put the new theory to the test by directly simulating the system that was measured in a recent study[3], i.e. a single *meso*-tetrakis-(3,5-di-tertiarybutylphenyl)-porphyrin ( $\text{H}_2\text{TBPP}$ ) molecule adsorbed on the silver (Ag) surface. The high resolution scanning tunneling microscope (STM) and Raman images[3] provide good references for theoretical modeling. The details of the density functional theory calculations are given in the Supplemental Material[17].

Here we considered two degenerate tautomers of  $\text{H}_2\text{TBPP}$  molecule[18]. The optimized structures of one  $\text{H}_2\text{TBPP}$  tautomer adsorbed on the Ag(111) surface are depicted in Fig. 1(a)[17]. The optimized structures of the other tautomers are similar except the central hydrogens bonded to different nitrogen atoms. We have considered three configurations: concave, plane, and convex, respectively. The first and last configurations were identified when  $\text{H}_2\text{TBPP}$  adsorbed on the Cu(111) surface by STM[19] and the second configuration is the minimum of the isolated molecule. Our calculations have shown that the concave is the most stable adsorption configuration, owing to the long range dispersion included in current calculations[20]. Meanwhile, the second stable configuration is the plane and the convex is the least stable one. The calculated STM images[17] of all configurations, together with the experimental result[3] are given in Fig. 1(b). One can immediately see that only the calculated STM image of the concave resembles well the experimental image. It can thus be concluded that  $\text{H}_2\text{TBPP}$  adsorbed on the Ag(111) surface has the concave configuration under the experimental conditions.

To simulate the Raman image,  $\text{H}_2\text{TBPP}$  was extracted from the optimized adsorption structures and its excited states were calculated by the time dependent density functional theory at the hybrid B3LYP level with 6-31G(d) basis sets[17]. It should be mentioned that it is the compromise that we have to make for such large systems from computational point of view. It is also a reasonable approximation since the molecule is only physisorbed on the Ag(111) surface. The strong absorption states for three configurations are found to be 2.47, 2.36, and 2.25 eV, respectively, in the region of the excitation energy of the experiment (532 nm, 2.33 eV)[3]. We have thus chosen these three excited states to simulate

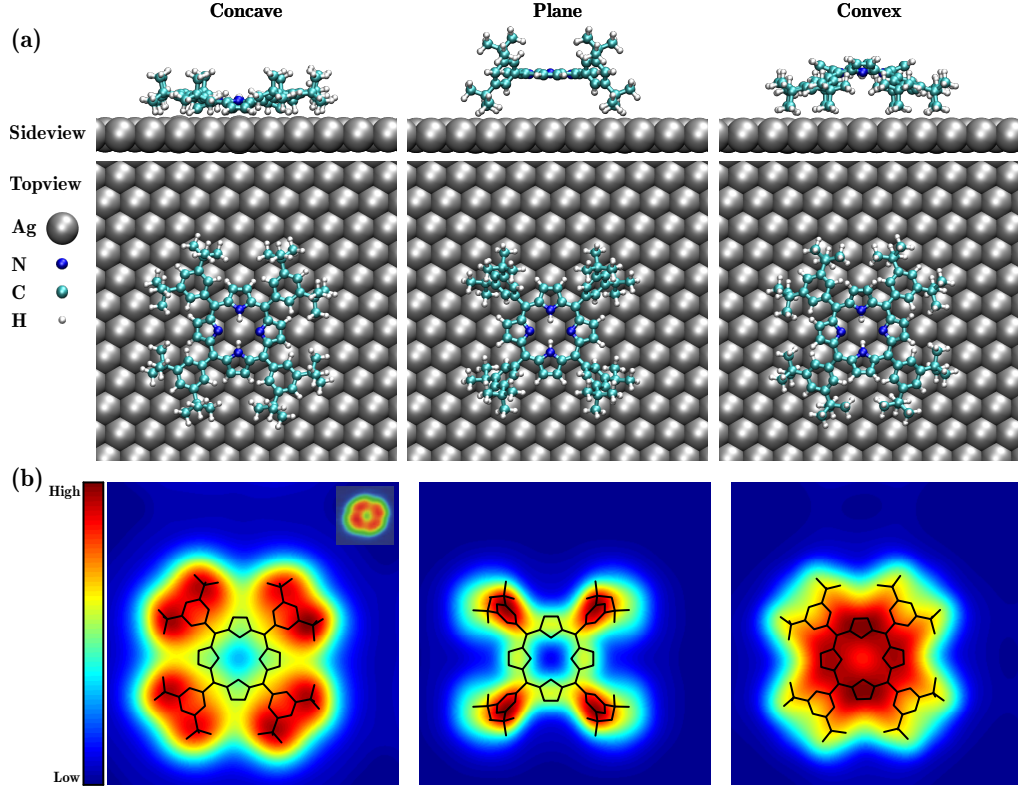


FIG. 1. (a) Optimized structures of one H<sub>2</sub>TBPP tautomer adsorbed on the Ag(111) surface for concave, plane, and convex configurations, respectively. Gray, blue, cyan and white balls represent Ag, N, C, and H atoms, respectively. Only the topmost slab layer of the Ag(111) surface as well as all atoms of adsorbates in one supercell are depicted for clarity. (b) Calculated average STM images with the sample biased by 1.0 V for concave, plane, and convex configurations, respectively. The solid lines represent the skeleton of H<sub>2</sub>TBPP. The insert figure shows the experimental STM image under the same condition extracted from Ref. 3.

the resonant Raman images. Consistent with the experimental setup[3, 21], the center of SCP, i.e.  $\mathbf{r}_D$ , is in the plane which is about 2 Å above the highest position of the adsorbates. Meanwhile, along the  $x$  and  $y$  directions, the full width at half maximum (FWHM) of the plasmonic field,  $g_{\alpha,D}^{000}$ , was set to be 5, 10, 20, and 30 Å, respectively, while the  $z$  component was fixed at 5 Å. We should emphasize that the calculated Raman images are not sensitive to small changes of  $\mathbf{r}_D$  and the  $\alpha$  in the  $z$  component of  $g_{\alpha,D}^{000}$ .

Under the resonant condition, for allowed transitions, the FC term  $P_{0,A}^L$  is known to be the dominant one[22]. All simulated linear Raman images from the FC term are presented in Fig. 2. It can be seen that the size of the Raman image is dependent on the size of the SCP. This implies that the precondition for the high resolution Raman image is to generate a highly focused plasmonic field. It is nice to observe that different configuration of the molecule gives very different Raman image, indicating that TERS technique is a powerful tool to study the structure of adsorbates. One can notice that the Raman image of the concave with FWHM of 20 Å is in very good agreement with the experimental image, which is

consistent with the energy and STM calculations. Here the symmetry breaking of the calculated Raman images should be attributed to the interaction between adsorbates and the Ag(111) substrate. By definition, Raman images reflect the density change involved in the electronic transition, rather than the local density of state of the adsorbate. This is naturally reflected by the obvious difference between the Raman and STM images.

The HT term  $P_{0,B}^L$  is dependent on the vibrational modes and its contribution can thus be used to identify the vibrations of the molecule. We have evaluated numerically the effect of the  $B$  term for two vibrational bands, around 820 and 1200 cm<sup>-1</sup>, by using the linear coupling model[23]. The calculated Raman images from the total polarization as well as the HT term alone for these two bands are shown in Fig. 3. One can immediately notice that the HT term is very sensitive to the vibrational modes. Its contribution to the total intensity holds the key to distinguish Raman images of different vibrations. For the H<sub>2</sub>TBPP molecule, the contribution of the HT term is very small. Hence, the Raman images from total intensity calculations appear to be identical for the two vibrational bands. It should be mentioned

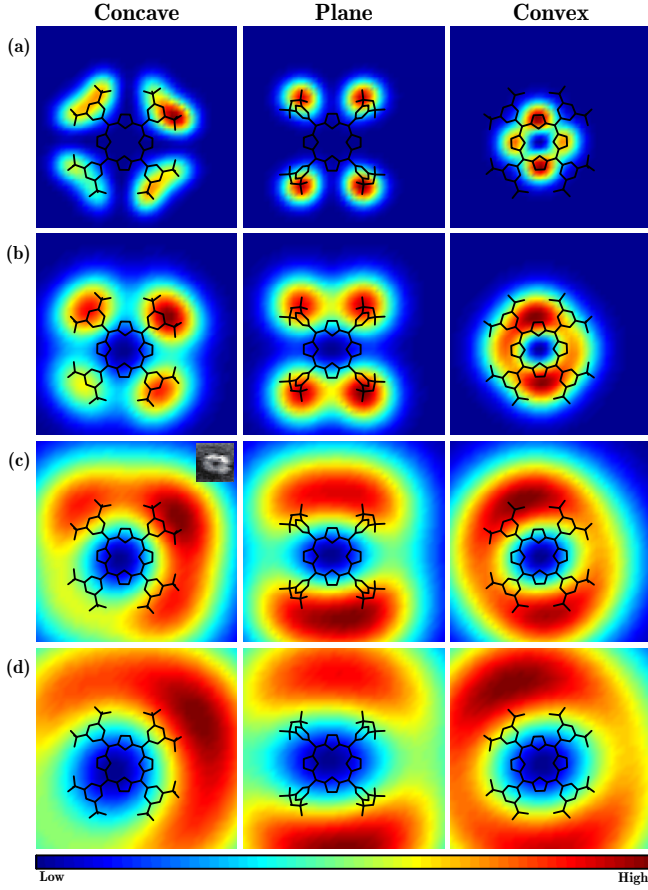


FIG. 2. Calculated linear Raman images from the FC term with the  $x$  and  $y$  components of full width at half maximum to be (a) 5 Å, (b) 10 Å, (c) 20 Å, and (d) 30 Å for concave, plane, and convex configurations, respectively. The solid lines represent the skeleton of H<sub>2</sub>TBPP, while, the insert figure shows the experimental Raman image extracted from Ref. 3.

that the Raman calculations are performed for the single molecule. The inclusion of the substrate could increase the contribution of the HT term. This could be a reason behind the small variation observed in the experimental Raman images[3]. We should emphasize that the calculated Raman images given in Ref. 3 were obtained by assuming that the confined plasmonic field does not alter the transition matrix itself, which is a simplified approximation to the basic theory presented in this work.

It was found experimentally that the observed Raman intensity was nonlinearly dependent on the power of the incident light[3]. The contributions of the linear and nonlinear processes to the total intensity were found to be 40% and 60%, respectively, at the saturation condition[3]. It is thus necessary to examine how the nonlinear process affects the Raman images of the molecule. Three processes, namely stimulated Raman as well as two hot luminescence processes (I and II), could contribute to the nonlinear Raman signal, when both pump and broadband SCPs are involved. In analogy to the theory pro-

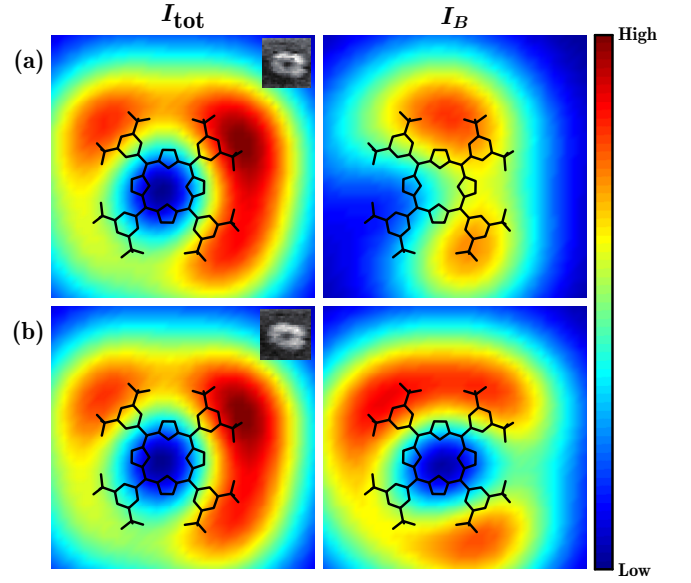


FIG. 3. Calculated linear Raman images of two bands at (a) 820 cm<sup>-1</sup> and (b) 1200 cm<sup>-1</sup> from total polarization ( $I_{\text{tot}}$ ) and only the HT term ( $I_B$ ) with the full width at half maximum of 20 Å for the concave configuration. The  $I_B$  was scaled by a factor of 100 and 400 for 800 and 1200 cm<sup>-1</sup>, respectively. The solid lines represent the skeleton of H<sub>2</sub>TBPP, while, the insert figures are the corresponding experimental Raman images extracted from Ref. 3.

posed by Lee *et al.*[7], the amplitude of induced nonlinear polarization also consists two terms

$$\mathbf{P}_0^{NL} = \mathbf{P}_{0,A}^{NL} + \mathbf{P}_{0,B}^{NL}, \quad (8)$$

where

$$\begin{aligned} \mathbf{P}_{0,A}^{NL} = & \frac{M_s^2 M_t |E_t^0|^3 \sqrt{2\pi} \tau_s}{\hbar^3} \langle \psi_r | \hat{\mathbf{r}} | \psi_g \rangle \langle \psi_r | \hat{\mathbf{r}} g(\mathbf{r}, \mathbf{R}_T) | \psi_g \rangle^3 \\ & \times \sum_{v^r, v^{r'}} \langle v^f | v^r \rangle \langle v^r | v^i \rangle \langle v^i | v^{r'} \rangle \langle v^{r'} | v^f \rangle \lambda^{(3)} + \text{NRT}. \end{aligned} \quad (9)$$

Here  $M_s$  is the enhancement factor of the broadband SCP that has the duration of  $2\sqrt{2\ln 2}\tau_s$ . The expression of  $\mathbf{P}_{0,B}^{NL}$  and the definition of  $\lambda^{(3)}$  could be found in Supplemental Material[17]. We would emphasize that  $\lambda^{(3)}$  is independent on the position of the TERS tip.

Similar to the linear process, the FC term is also completely dominant in the nonlinear process. Once the  $\mathbf{P}_0^{NL}$  is obtained,  $|\mathbf{P}_0^L|^2$  in Eq. 5 could be replaced by  $|\mathbf{P}_0^{NL}|^2$  or their summation for nonlinear or total Raman intensities, respectively, because the phases of them are unrelated[24]. Admittedly, obtaining the absolute value of linear and nonlinear polarizations requires the solution of the classical Maxwell's equations for realistic nanostructures. Instead, we use the experimentally determined contributions of the linear and nonlinear terms in the saturation condition[3] to define the pre-factors.

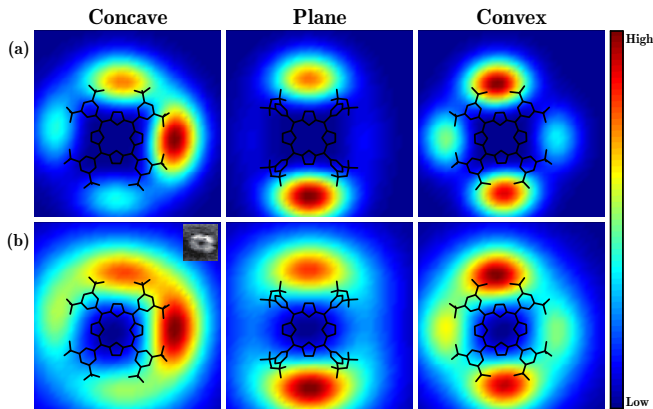


FIG. 4. Calculated (a) nonlinear and (b) total Raman images for concave, plane, and convex configurations, respectively, under the plasmonic field with the full width at half maximum of 20 Å. The solid lines represent the skeleton of H<sub>2</sub>TBPP, while, the insert figure shows the experimental Raman image extracted from Ref. 3.

The calculated nonlinear Raman images with FWHM of 20 Å are depicted in Fig. 4(a). In general, the nonlinear images do have higher spatial resolution than their linear counterparts. However, for this particular system, the improvement is not as much as one anticipated[3]. The calculated total Raman image (including both linear and nonlinear effects) from the concave configuration with the field distribution size of 20 Å, gives the best agreement with the experimental image as shown in Fig. 4(b). This result reveals that the actual size of the experimentally confined plasmonic field could be close to 20 Å, which is consistent with our numerical EM simulations[17] and may be the decisive factor for the sub-nanometer Raman images. However, the increase of the nonlinear contribution to the total intensity will on the other hand be an effective way to further improve the resolution of the Raman image.

In summary, we have proposed a quantum mechanical description for the interaction between a molecule and a highly confined plasmonic field. It shows that the SCP could modify the transition matrix and result in the Raman images with high resolution. The usefulness of the description is highlighted by reproducing successfully the experimental Raman images of a H<sub>2</sub>TBPP molecule adsorbed on the Ag(111) surface. The theoretical framework established in this work lays the foundation for the future development of linear and nonlinear plasmonic spectroscopy.

This work was supported by the Ministry of Science and Technology of China (2010CB923300), Natural Science Foundation of China (21121003), Strategic Priority Research Program of Chinese Academy of Sciences (XDB01020200), Göran Gustafsson Foundation for Re-

search in Natural Sciences and Medicine, and the Swedish Research Council (VR). The Swedish National Infrastructure for Computing (SNIC) was acknowledged for computer time.

\* yiluo@ustc.edu.cn

- [1] R. M. Stöckle, Y. D. Suh, V. Deckert, and R. Zenobi, *Chem. Phys. Lett.* **318**, 131 (2000).
- [2] B. Pettinger, B. Ren, G. Picardi, R. Schuster, and G. Ertl, *Phys. Rev. Lett.* **92**, 096101 (2004).
- [3] R. Zhang, Y. Zhang, Z. C. Dong, S. Jiang, C. Zhang, L. G. Chen, L. Zhang, Y. Liao, J. Aizpurua, Y. Luo, J. L. Yang, and J. G. Hou, *Nature* **498**, 82 (2013).
- [4] D. A. Long, *The Raman Effect: A Unified Treatment of the Theory of Raman Scattering by Molecules* (Wiley, Chichester New York, 2002).
- [5] M. O. Scully and M. S. Zubairy, *Quantum Optics*, 1st ed. (Cambridge University Press, Cambridge New York, 1997).
- [6] A. C. Albrecht, *J. Chem. Phys.* **34**, 1476 (1961).
- [7] S.-Y. Lee, D. Zhang, D. W. McCamant, P. Kukura, and R. A. Mathies, *J. Chem. Phys.* **121**, 3632 (2004).
- [8] E. M. Purcell, *Phys. Rev.* **69**, 681 (1946).
- [9] J. Neugebauer, M. Reiher, C. Kind, and B. A. Hess, *J. Comput. Chem.* **23**, 895 (2002).
- [10] E. Le Ru and P. Etchegoin, *Principles of Surface-Enhanced Raman Spectroscopy: and Related Plasmonic Effects*, 1st ed. (Elsevier, Amsterdam Boston, 2009).
- [11] A. Archambault, F. Marquier, J.-J. Greffet, and C. Arnold, *Phys. Rev. B* **82**, 035411 (2010).
- [12] H. Xu, X.-H. Wang, M. P. Persson, H. Q. Xu, M. Käll, and P. Johansson, *Phys. Rev. Lett.* **93**, 243002 (2004).
- [13] P. Johansson, H. Xu, and M. Käll, *Phys. Rev. B* **72**, 035427 (2005).
- [14] J. K. Sass, H. Neff, M. Moskovits, and S. Holloway, *J. Phys. Chem.* **85**, 621 (1981).
- [15] E. J. Ayars, H. D. Hallen, and C. L. Jahncke, *Phys. Rev. Lett.* **85**, 4180 (2000).
- [16] T. Iwasa and K. Nobusada, *Phys. Rev. A* **80**, 043409 (2009).
- [17] See Supplemental Material for theoretical background, computational details, and EM field simulations.
- [18] Q. Fu, J. Yang, and Y. Luo, *App. Phys. Lett.* **95**, 182103 (2009).
- [19] S. Ditze, M. Stark, F. Buchner, A. Aichert, N. Jux, N. Luckas, A. Görling, W. Hieringer, J. Hornegger, H.-P. Steinrück, and H. Marbach, *J. Am. Chem. Soc.* **136**, 1609 (2014).
- [20] S. Grimme, *J. Comput. Chem.* **27**, 1787 (2006).
- [21] X. H. Qiu, G. V. Nazin, and W. Ho, *Science* **299**, 542 (2003).
- [22] A. Myers Kelley, *J. Phys. Chem. A* **112**, 11975 (2008).
- [23] P. Macak, Y. Luo, and H. Ågren, *Chem. Phys. Lett.* **330**, 447 (2000).
- [24] D. S. Chemla, *Rep. Prog. Phys.* **43**, 1191 (1980).